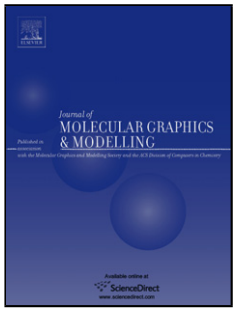

Title: Nonlinear optical properties of rhenium (I) complexes: influence of the extended π-conjugated connectors and proton abstraction

Author: Hai-Ling Yu Bo Hong Ning Yang Hong-Yan Zhao

PII: S1093-3263(15)30031-0
DOI: http://dx.doi.org/doi:10.1016/j.jmgm.2015.07.008
Reference: JMG 6580

To appear in: *Journal of Molecular Graphics and Modelling*

Received date: 26-4-2015
Revised date: 20-7-2015
Accepted date: 22-7-2015

Please cite this article as: H.-L. Yu, B. Hong, N. Yang, H.-Y. Zhao, Nonlinear optical properties of rhenium (I) complexes: influence of the extended *rmpi*-conjugated connectors and proton abstraction, *Journal of Molecular Graphics and Modelling* (2015), http://dx.doi.org/10.1016/j.jmgm.2015.07.008

Graphical abstract

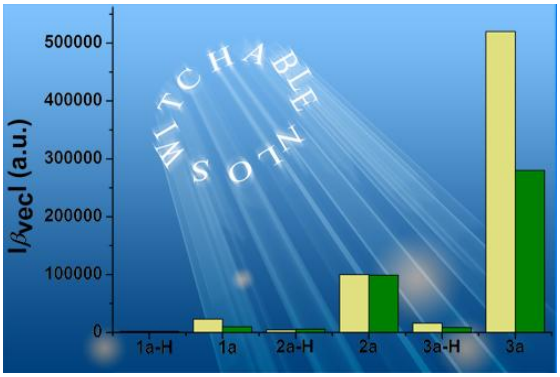

The switchable NLO responses of series of rhenium (I) complexes have been systematically investigated by density functional theory. The first hyperpolarizabilities (β_{vec}) increase remarkably with further extending of the organic connectors. The enhancement is due to the better delocalization of the π-electron system and the more obvious degree of charge transfer.

Highlights

- ► Deprotonation affect causes an efficient second-order NLO switching
- ► Deprotonation has an influence on the β_{vec} sign from positive to negative
- ► The differences on NLO properties are due to a change in charge transfer pattern
- ► The absorption bands of all complexes show deprotonation dependence

Nonlinear optical properties of rhenium (I) complexes: influence of the extended π-conjugated connectors and proton abstraction

Hai-Ling Yu [a], Bo Hong [a,*], Ning Yang [a], Hong-Yan Zhao [b,*]

[a] *College of Resources and Environmental Science, Jilin Agricultural University, Changchun, Jilin 130024, People's Republic of China*

[b] *State Environmental Protection Key Laboratory of Wetland Ecology and Vegetation Restoration, Northeast Normal University, Changchun, Jilin 130024, People's Republic of China*

Abstract

The photoinduced proton-coupled electron transfer chemistry is very crucial to the development of nonlinear optical (NLO) materials with large first hyperpolarizability contrast. We have performed a systematic investigation on the geometric structures, NLO switching, and simulated absorption spectra of rhenium (I) complexes via density functional theory (DFT). The results show that the first hyperpolarizabilities (β_{vec}) increase remarkably with further extending of the organic connectors. In addition, the solvent leads to a slight enhancement of the hyperpolarizability and frequencydependent hyperpolarizability. Furthermore, the proton abstraction plays an important role in tuning the second-order NLO response. It is found that deprotonation not only increases the absolute value of β_{vec} but also changes the sign of β_{vec} from positive to negative. This different sign can be explained by the opposite dipole moments. The efficient enhancement of first hyperpolarizability is attributed to the better delocalization of the π-electron system and the more obvious degree of charge transfer. Therefore, these kinds of complexes might be promising candidates for designed as proton driven molecular second-order NLO switching.

* Corresponding Author.
Fax: (+86) 431 85098072(H.Y. Zhao)
E-mail addresses: hyzhao@nenu.edu.cn (H.Y. Zhao), Jlauhb@163.com

Key words: Re (I) complex; Deprotonation; NLO property; Molecular switching; DFT

1. Introduction

In recent years, the design and synthesis of non-linear optical (NLO) molecular materials have attracted considerable attention due to their unique applications in optical fiber, data storage, and signal processing [1-4]. Comparing with traditional organic chromophores, the transition metal molecules play important roles in NLO activities. Because they exhibit large and fast NLO activities by charge-transfer transitions between the metal and ligands [5-8]. The transition metal complexes Ru (II), Fe (II), Pt (II), Re (I) and Ni (II) have shown versatile second-order NLO properties [9-13]. For example, Ordronneau et al. have reported that the β value of the Re (I) dithienylethene complex increases about 5-fold through reversible photoisomerization process, which achieves a switchable NLO response [14]. Then, the effect of metal chelation on various push-pull ligands such as substituted pyridines [15], phenanthroline [16], and dithiolene [17] has been extensively studied. Especially, the substituted phenanthroline and pyridine ligands show the excellent chelating ability [18]. When these ligands are coordinated to the metal center, the chelation prompts them to adopt plane arrangement, which is favorable for large second-order NLO response [19, 20].

For metal complexes, they are conducive to efficiently switching the second-order NLO responses at the molecular level, which could provide the basis for a range of molecular-scale devices [21, 22]. To obtain the effective switching of the molecular first hyperpolarizability, the prerequisite is that a molecule must exist at least two stable states [23]. Specific methods including redox, protonation, and photocyclization have been employed to switch the NLO responses [24-26]. Among them, the more appealing schemes are redox and protonation, since they can lower the donor/acceptor capacity of the typical donor-acceptor significantly (D-A) [27, 28].

Recently, series of Re (I) complexes were synthesized and investigated, in which the phenol unit is linked covalently to the tricarbonyl-(phenanthroline) (pyridine)rhenium (I) via a variable number of benzene rings spacers (n = 0-2) [29], that is, $[Re(phen)(CO)_3(py\text{-}phOH)]^+$ (phen = 1,10-phenanthroline; CO = carbonyl; py-phOH = phenolate-pyridine) (Fig. 1). Besides, the phenolate moieties of the Re (I) complexes can underwent reversible deprotonation-protonation processes, which provides the possibility for the molecular NLO switching. In the present work, the protonated forms are named as **1a-H** to **3a-H**, while the corresponding deprotonated forms are **1a-3a** (Fig. 1). We have also investigated the influence of π-conjugated connectors (by changing the number of benzene rings) on the second-order NLO response.

2. Computational details

All of the calculations were carried out using the Gaussian 09W program package [30]. It is well-know that B3LYP method shows good accuracy to optimize the geometries of the medium-sized molecules [31]. Thus, all complexes were optimized at the B3LYP/6-31G(d) (LANL2DZ basis set for Re ion) level without symmetry constraint. At the same level of theory, natural bond orbital (NBO) analysis was performed at the B3LYP/6-31+G(d)/LanL2DZ level. To further understand the bonding character of complexes, we evaluated the wiberg bond index (WBI) using NBO analysis. The electrostatic potential (ESP) and electron density analysis was performed by Multiwfn 3.5 software [32]. The ESP was plotted using VMD 1.9.1 [33]. According to the reference [34], the proton binding energy, ΔE_{H+}, is defined as:

$$\Delta E_{H^+} = (E\{Re(I)(phen)(CO)_3(py\text{-}phO)\} + ZPE\{Re(I)(phen)(CO)_3(py\text{-}phO)\}) - (E\{[Re(I)(phen)(CO)_3(py\text{-}phOH)]^+\} + ZPE\{[Re(I)(phen)(CO)_3(py\text{-}phOH)]^+\}) \quad (1)$$

Where

$(E, ZPE)\{Re(I)(phen)(CO)_3(py\text{-}phO)\}$ and $(E, ZPE)\{[Re(I)(phen)(CO)_3(py\text{-}phOH)]^+\}$ are the electronic energies and zero-point energies of the optimized complexes, respectively.

The static first hyperpolarizabilities of the studied complexes were calculated by

analytical third energy derivatives, which are more efficient and less expensive [35, 36]. For dipolar molecules, the first hyperpolarizability is generally related to the β_{vec} value, which is the vector component of β along the dipole moment direction and given by the following:

$$\beta_{vec} = \sum_{i=x,y,z} \frac{\mu_i \beta_i}{|\mu|} \tag{2}$$

where β_x, β_y, and β_z represent the components of the first hyperpolarizability tensor along *x*-, *y*-, and *z*-axis, respectively. Here, μ is the ground-state dipole moment, β_i is defined by the equation:

$$\beta_i = \beta_{iii} + \frac{1}{3}\sum_{j \neq i}\left(\beta_{ijj} + \beta_{jij} + \beta_{jji}\right) \quad i, j = x, y, z \tag{3}$$

To check the consistency of results, we have calculated the first hyperpolarizabilities using three functionals, including hybrid exchange-correlation B3LYP, long-range corrected functionals LC-BLYP and CAM-B3LYP. The long-range corrected (LC) XC functional, LC-BLYP [37, 38] with a range-separating parameter μ of 0.47, furthermore, LC-BLYP contains 100% of HF exchange in the long-range limit. Among them, LC XC functionals have been shown to correct conventional DFT schemes for their shortsighted drawbacks [39]. The BLYP method is based purely on Kohn-Sham DFT formalism, combining the standard slater local exchange functional with the exchange gradient-corrected Becke and the Lee-Yang-Parr correlation functional [40]. The CAM-B3LYP functional [41], which adds a long-range correction using the Coulomb-attenuating method and includes 19% and 65% of short- and long-range HF exchange with μ=0.3, is suitable to predict the molecular NLO properties of large systems. In addition, the PCM model has been used to examine the solvent effect on the first static hyperpolarizabilities and frequency-dependent hyperpolarizabilities.

In order to elucidate the origin of second-order NLO properties, we employed time-dependent density functional theory (TD-DFT) to descript the electronic spectra. The TD-DFT method is one of the most successful and extensively used methods to calculate the excitation energies in quantum chemistry owing to its efficiency and

accuracy. To choose suitable calculated methods, the electron absorption spectrum of complexes **1a-H** and **2a-H** was simulated using TD-CAM-B3LYP and TD-PBE1PBE methods with 6-31+G(d) (LANL2DZ basis set for Re ion) basis set associated with the polarized continuum model (PCM) in acetonitrile solution (Table S1). According to the results, absorption spectrum of complex **1a-H** contains one high-energy electronic transition absorbing at 287 nm along with a low-energy electronic transition at 298 nm, which tally with the experiment result [29]. Similarly, absorption spectrum of complex **2a-H** contains one high-energy electronic transition absorbing at 284 nm along with a low-energy electronic transition at 299 nm. Thus, the TD-CAM-B3LYP functional was selected for the simulation of the absorption spectra of the studied complexes.

3. Results and discussion

3.1. Geometric and electronic structure

As shown in Fig. 1, the Re is coordinated by three carbonyl, one pyridine, and one phenanthroline ligand to form an almost perfect octahedral coordination polyhedron. The initial geometric structure of complex **2a-H** is derived from X-ray crystal data. The calculated geometric parameters of complex **2a-H** at the B3LYP/6-31G(d) level are in reasonable agreement with reported experimental data (Table 1). To obtain more accurate geometry, solvent effect has been taken into account in optimization and modeled using the polarized continuum model (PCM). We also optimized the geometrical structure of complex **2a-H** in the acetonitrile solution (Table 1). It can be clearly observed that the deviation of the calculated bond lengths (≤0.002 Å) and bond angles (≤1.99°) for complex **2a-H** based on the B3LYP method in vacuum or acetonitrile solution is very small and negligible. Hence, the geometric structures and electronic properties of all complexes have been computed in vacuum at the B3LYP/6-31G(d) level with real frequency. The results show that both the (Re-N, Re-C) distances and (N-Re-N, N-Re-C, and C-Re-C) angles are slightly effected (in

range of 0.001-0.019Å and <5°, respectively) during the deprotonation process. This means that the abstraction of proton from the phenolate-pyridine moiety has a slightly effect on the configuration of the studied complexes. In order to further understand the geometrical structures of complexes, we calculated the bond length alternation (BLA, the difference between single and double bond lengths) between pyridine and phenol unit. It is obvious that the trend of the BLA values of the protonated complexes is consistent with those of the deprotonated complexes. However, the BLA values of the deprotonated forms are smaller than those of the corresponding protonated forms, which implies the enhanced conjugation of phenolate-pyridine moiety during the deprotonation process. Moreover, as increasing the number of benzene rings between pyridine and phenol units, the BLA values of the studied complexes become smaller, supporting the gradually better conjugation. These changes in the geometries may be beneficial to the enhancement of the second-order NLO properties.

In order to discuss the bonding characteristics between metal and ligand, the natural bond orbital (NBO) was analysis. Fig. 2 shows the local molecular orbitals of Re−N bonds of experimental **2a-H** and **2a**. It is found that the Re−N1 bonds are formed from the $5d_{z2}$ (Re) and $2p_z$ (N) orbital. Meanwhile, the σ Re−N2 (N3) bonds are formed from $5d_{xy}$ (Re) and $2p_x$ (N) orbital. The Re−N bonds of complex **2a-H** are similar to those of **2a**. The results indicate that the deprotonation process has a minimal effect on the bond characteristic between the metal and ligand, which is agreed with the slight variation of Re-N bond lengths during the deprotonation process.

The proton binding energy (ΔE_H^+) is a sensitive indicator to detect the ability of removing a proton from the titled molecule. The larger the ΔE_H^+ value means the more difficult to remove the proton from the molecule. The ΔE_H^+ values of complexes **1a-3a** increase gradually with the extension of π-conjugated connectors (ΔE_H^+ is 270.27, 286.35, and 291.25 kcal/mol, respectively). So why does the introducing of the extensive connectors induce the large proton binding energy? In fact, for protonated species, the bond lengths follow the order of O-H (**1a-H**) > O-H (**2a-H**) >

O-H (**3a-H**). And the order of WBI is WBI (**3a-H**) > WBI (**2a-H**) > WBI (**1a-H**), indicating that the bond strength (O-H) of **3a-H** is stronger than that of **1a-H** and **2a-H** (Table 1). The shorter bond length and stronger bond strength indicate the larger proton binding energy for O-H. In addition, the electron density and energy density of the critical point (where gradient norm of function value is zero) were calculated on the basis of atoms in molecules (AIM) theory. Results show that the electron density around the O-H bond (Table 2) also exhibits the same trend of proton binding energy. On the other hand, the delocalized region of π electrons increases with extending π-conjugated connectors from **1a-H** to **3a-H**, which might increase the proton binding strength. This illustrates that the further extending of the organic connectors at the phenolate-pyridine moieties is unfavorable to improve the deprotonation ability.

3.2. The dipole moment and static first hyperpolarizability

It is instructive to study the dipole moments (μ), which is more directly related to the β_{vec} value. As shown in Table 3, for the protonated complexes, the dipole moments are contributed by μ_x and μ_z components. However, the protonation leads to a large variation of the dipole moment component μ_z. As a result, the μ for the deprotonated complexes are mainly decided by the *z*-axis, that is, $\mu \approx \mu_z$. For protonated species, there is no obvious change on dipole moments. However, for deprotonated species, the dipole moments of complexes **1a-3a** increase progressely with the gradual extension of π-conjugated connectors, which can be explained by the ESP (the Cartesian coordinate system is located at the middle of the Re and the transversal *z*-axis points to phenolate-pyridine moiety and the longitudinal *x*-axis points to the phenanthroline moiety). As shown, the complexes **1a-3a** show similar distribution of ESP (Fig. 3). Therefore, a further increase of conjugation along the *z*-axis increases the dipole moments. Further, the sign of the μ_z values of protonated species are opposite to those of deprotonated species. It further explains why the sign of β_{vec} in deprotonated form is negative.

Choosing an appropriate method to calculate the first hyperpolarizabilities of the

molecules is crucial. It is worth noting that DFT included electron correlation effects appears as the natural alternative for computing the first hyperpolarizabilities of large-size complexes at low computational costs [42, 43]. In this paper, the first hyperpolarizabilities were calculated using the Lee-Yang-Parr correlation functional B3LYP, CAM-B3LYP and LC-BLYP functionals at 6-31+G(d) the basis set (Table 3 and Table S2). Additionally, the β_{vec} values of the systems are functional-dependent, and three functionals show the same trend. Then, we will discuss the trend of the β_{vec} values at the CAM-B3LYP functional. It is clearly found that the β_z component has the largest contribution to the β_{vec} value, which is in line with the main charge transfer along the *z* direction (see the related discussion in the absorption spectra section). Note that the order of the β_{vec} values is β_{vec} (**1a-H**) < β_{vec} (**2a-H**) < β_{vec} (**3a-H**). To be specific, β_{vec} value of complex **1a-H** is 2.0×10^3 a.u.. And complexes **2a-H** and **3a-H** possess large β_{vec} values (4.5×10^3 a.u., 1.6×10^4 a.u., respectively), which are ~3 and ~ 8 times as large as complex **1a-H**. The same trend of β_{vec} values is found in deprotonated species, that is, β_{vec} (**1a**) < β_{vec} (**2a**) < β_{vec} (**3a**). It indicates that the β_{vec} values have a progressively enhancement with the extension of the π-conjugated connecter. More interestingly, the β_{vec} sign of the protonated and deprotonated species is opposite, which must be related to the change of dipole moment and charge transfer pattern. The solvent effect is also taken into account for the static first hyperpolarizabilitiy in acetonitrile solution by CAM-B3LYP functinonal (see Table 3). The results show that the first hyperpolarizabilities are in the range of ~1.1 to ~1.8 times larger than that of calculations in vacuo. However, the order of the first hyperpolarizabilities for the protonated complexes is still in accord with the results in vacuo.

According to Table 3, the deprotonation process is associated with a remarkably large first hyperpolarizability contrast. Here, the ratio of β_{vec} values (β_{vec}(**a-H**)/β_{vec}(**a**)) is employed to measure the switchable effect. For example, the difference on the β_{vec} values for system **1** from protonated (**1a-H**) to deprotonated form (**1a**) is the smallest, which is β_{vec}(**1a**) =5β_{vec}(**1a-H**). In addition, the meaningful switchable results occur at system **2** and **3** with their larger β_{vec} ratio (β_{vec}(**2a**) =22β_{vec}(**2a-H**) and β_{vec}(**3a**)

=32β_{vec}(**3a-H**), respectively). This is attributed to the enhanced conjugation in the *z*-axis, because the BLA values of the deprotonated complexes are all smaller than those of the corresponding protonated complexes. Thus, it can be concluded that the switchable NLO can be obtained by the deprotonation process in these complexes.

To have an insight into the origin of second-order NLO responses, we consider the widely used two-level model established by Oudar and Chemla [44]. In the two-level model expression, the first hyperpolarizability is proportional to the oscillator strength (f_{os}) and inversely proportional to the third power of the transition energy (E_{ge}). It is considered that the low transition energy is the decisive factor for β_{vec} value. We listed the E_{ge} values at the crucial transition states (with the largest oscillator strengths) in Table 4. The crucial transition energies show a descending trend with the gradually extension of the π-conjugated connecter: **1a-H** (3.86 eV) > **2a-H** (3.82 eV) > **3a-H** (3.78 eV), **1a** (3.12 eV) > **2a** (2.77 eV) > **3a** (2.33 eV). It illustrates that the insertion of organic connectors between the phenolate-pyridine moieties significantly alters the first hyperpolarizabilities (Fig. 4). These decreasing trends are consistent with those of the deprotonation process: **1a-H** (3.86 eV) > **1a** (3.12 eV), **2a-H** (3.82 eV) > **2a** (2.77 eV), **3a-H** (3.78 eV) > **3a** (2.33 eV). Therefore, deprotonation process could significantly switch the second-order NLO responses of the studied complexes, and the Re (I) complexes can act as the efficient second-order NLO switching materials.

3.3. Frequency-dependent first hyperpolarizability

The experimental measurement of hyperpolarizabilities usually involves oscillating electric fields. It is of great importance to determine the frequency-dependent properties theoretically. $\beta(-2\omega;\omega,\omega)$ is the second harmonic generation (SHG) and measured in a fundamental incident wavelength. The incident wavelength should have a second harmonic far enough from the absorption bands to avoid the overmeasure of the β values due to resonance effects [45, 46]. Therefore, we investigated the frequency dependent first hyperpolarizabilities at a nonresonant wavelength of 1.064 μm (ω = 0.0428 eV). The $\beta(-2\omega;\omega,\omega)$ was calculated by the coupled-perturbed DFT at

the CAM-B3LYP/6-31+G(d) level (Table 5). As compared with the static first hyperpolarizability, the frequency dispersion at 1.064 μm leads to 1.0, 1.0, 1.1 times increases for complexes **1a-H** to **3a-H** but 1.1, 1.5, 1.8 times enhancement for complexes **1a-3a**, respectively. The β (-2ω;ω,ω) value of **3a** is considerable larger compared with the static β_{vec} value, which may be due to a resonant around second harmonic with the weak absorption at 450nm. Meanwhile, the frequency-dependent hyperpolarizabilities in acetonitrile solution were calculated using CPDFT method with CAM-B3LYP functional for all complexes. As shown in Table 5, the solvent also leads to a slight enhancement of the frequency-dependent hyperpolarizability for each complex relevant to its frequency-dependent hyperpolarizability in vacuo.

3.4. Absorption spectrum

In order to obtain a more intuitive description of the band assignments of the electronic absorption spectra and the trend of the NLO behaviors, the orbital features involved in the crucial excitation for the studied complexes have been shown (Fig. 5). The absorption spectrum contains three absorption peaks: the low-energy, middle-energy, and high-energy regions. In our work, the simulation absorption parameters are derived from the TDDFT calculation using the Gaussian 09W program package [47]. The data were dealed with by Gauss-Sum2.2.5. The absorption spectra charts were plotted using the origin8.5 software.

According to the two-level model, the first hyperpolarizability is related to the low-energy crucial excitation. Hence, we only considered the charge transfer transitions of the low-energy peaks. Complexes **1a-H** and **2a-H** have a maximum absorption at low-energy region (298 nm and 299 nm, respectively) (Fig. 5). It is obvious that the electron transitions of HOMO-1→LUMO of complexes **1a-H** and **2a-H** are both categorized as ligand-to-ligand charge transfer (LLCT) [π(phenolate) → π*(phen)]. The HOMO -1 is mainly delocalized on the phenolate-pyridine moiety, while the LUMO is mainly located at the phenanthroline moiety (Fig. 5). Compared with complex **1a-H** and **2a-H**, complex **3a-H** shows the bathochromic shift of the

maximum absorption together with an increasing intensity. The low-energy absorption of all complexes show LLCT [π(phenolate) → π*(phen)]. With exception of this kind of charge transfer, the low-energy absorption of complex **3a-H** also can be viewed as π → π* transition from phenmethyl to phen fragments, which is along the negative *z*-axis and is responsible for the β_z component (Fig. 6). Obviously, increasing the number of benzene rings has an efficient increase on the charge transfer (CT) degree of all protonated complexes, which results in an effective enhancement of the β_{vec} values.

Similar spectra characters have been obtained with the deprotonated species (**1a-3a**) (Fig. 5). Compared with protonated species, obvious red-shift is found in the low-energy absorption at 396 nm, 446 nm and 459 nm. The red shift of band is helpful for enhancing the NLO responses. The low-energy electronic transition arises from the HOMO → LUMO+2 excitations. Since the HOMO-1 is delocalized over the whole phenolate-pyridine moiety, there is no doubt that the HOMO → LUMO+2 of complexes **1a-3a** are all ascribed as the intraligand charge transfer (ILCT) [π(py-phOH) → π*(py-phOH)]. As compared with protonated species, there is obvious overlap between the orbitals of HOMO and LUMO+2, reflecting the ease in the electronic transition. This easy transition is responsible for the lower transition energy, thus, enhancing the nonlinear optical property of complexes **1a-3a**.

4. Conclusions

The geometrical structures and second-order NLO properties of series pincer Re (I) complexes with their corresponding deprotonated species were investigated by DFT methods. The bond length between Re and N atom has little change during the deprotonation process. The NBO calculation suggests that the Re-N bonds are formed from the $5d_{z2}$ (Re), $5d_{xy}$ (Re), $2p_x$ (N) and $2p_z$ (N) orbital. According to the calculated ΔE_H^+ value, further extending of the organic connectors at the phenolate-pyridine moieties is unfavorable for the improvement of the deprotonation ability. However, extending the organic connectors can enhance the second-order NLO response.

During the deprotonation process, 5-, 22-, 32-fold switching ratio can be discovered for systems **1**-**3**, respectively. The deprotonation reactions can obviously decrease transition energies, which is useful for these complexes to be designed as proton driven molecular second-order NLO switching. Also, the deprotonation reactions results in red shift for absorption spectra due to the change in electron distribution. Our studies provide new insights into the photoinduced proton-coupled electron transfer chemistry, particularly with respect to the importance of strong electronic coupling between the donor and acceptor units.

Supplementary data

Main absorption wavelengths λ (nm) of complexes **1a-H** and **2a-H**. Dipole moments and static first hyperpolarizabilities β_{vec} (a.u.) of all complexes (B3LYP/6-31+G(d)).

Acknowledgments

The authors gratefully acknowledge the financial support from the Natural Science Foundation of China (No. 41471165) and the National Science Foundation of Jilin(No. 20130101081JC). In addition, this study was supported by the Jilin Province Science and Technology Department of Science and Technology Development Program (20110952 and 20130102078JC). We are grateful to the Faculty of Chemistry of Northeast Normal University for computing resource.

References

[1] J.P. Costes, J.F. Lamère, C. Lepetit, P.G. Lacroix, F. Dahan, Synthesis, crystal structures, and nonlinear optical (NLO) properties of new schiff-base Nickel(II) complexes. toward a new type of molecular switch? Inorg. Chem. 44 (2005) 1973-1982.

[2] B.J. Coe, Switchable nonlinear optical metallochromophores with pyridinium electron acceptor groups, Acc. Chem. Res. 39 (2006), 383-393.

[3] S. Di Bella, I. Fragalà, I. Ledoux, M.A. Diaz-Garcia, T.J. Marks, Synthesis, characterization, optical spectroscopic, electronic structure, and second-order nonlinear optical (NLO) properties of a novel class of donor−acceptor bis(salicylaldiminato)nickel(II) schiff base NLO chromophores, J. Am. Chem. Soc. 119 (1997) 9550-9557.

[4] M. Nakano, T. Minami, K. Yoneda, S. Muhammad, R. Kishi, Y. Shigeta, T. Kubo, L. Rougier, B. Champagne, K. Kamada, K. Ohta, Giant enhancement of the second hyperpolarizabilities of open-shell singlet polyaromatic diphenalenyl diradicaloids by an external electric field and donor–acceptor substitution, J. Phys. Chem. Lett. 2 (2011) 1094-1098.

[5] C.G. Liu, X.H. Guan, Computational Study on redox-switchable second-order nonlinear optical properties of totally inorganic keggin-type polyoxometalate complexes, J. Phys. Chem. C 117 (2013) 7776-7783.

[6] S. Muhammad, H.L. Xu, Z.M. Su, Capturing a synergistic effect of a conical push and an inward pull in fluoro derivatives of $Li@B_{10}H_{14}$ basket: toward a higher vertical ionization potential and nonlinear optical response, J. Phys. Chem. A 115 (2011) 923-931.

[7] W.Y. Wang, N.N. Ma, C.H. Wang, M.Y. Zhang, S.L. Sun, Y.Q. Qiu, Enhancementof second-order nonlinear optical response in boron nitride nanocone: Li-doped effect, J. Mol. Graphics. Modell. 48 (2014) 28-35.

[8] M. Malaun, Z.R. Reeves, R.L. Paul, J.C. Jeffery, J.A. McCleverty, M.D. Ward, I. Asselberghs, K. Clays, A. Persoons, Reversible switching of the first hyperpolarisability of an NLO-active donor–acceptor molecule based on redox interconversion of the octamethylferrocene donor unit, Chem. Commun. 01 (2001) 49-50.

[9] M. Halter, Y. Liao, R.M. Plocinik, D.C. Coffey, S. Bhattacharjee, U. Mazur, G.J. Simpson, B.H. Robinson, S.L. Keller, Molecular self-assembly of mixed high-beta zwitterionic and neutral ground-state NLO chromophores, Chem. Mater. 20 (2008)

1778-1787.

[10] H. Fukui, S. Takamuku, T. Yamada, K. Fukuda, T. Takebayashi, Y. Shigeta, R. Kishi, B. Champagne, M. Nakano, Open-shell character and second hyperpolarizabilities of one-dimensional Chromium(II) chains: size dependence and bond-length alternation effect, Inorg. Chem. 53 (2014) 8700-8707.

[11] A. Breivogel, S. Wooh, J. Dietrich, T. Yon Kim, Y. Soo Kang, K. Char, K. Heinze1, Anchor-functionalized push-pull-substituted bis(tridentate) Ruthenium(II) polypyridine chromophores: photostability and evaluation as photosensitizers, Eur. J. Inorg. Chem. 16 (2014) 2720-2734.

[12] M. Nakano, T. Minami, K. Yoneda, S. Muhammad, R. Kishi, Y. Shigeta, giant enhancement of the second hyperpolarizabilities of openshell singlet polyaromatic diphenalenyl diradicaloids by an external electric field and donor–acceptor substitution, J. Phys. Chem. Lett. 2 (2011) 1094-1098.

[13] A. Rana, S. Lee, D. Kim, P. K. Panda, β-Octakis(methylthio)porphycenes: synthesis, characterisation and third order nonlinear optical studies, Chem. Commun. 51 (2015) 7705-7708.

[14] L. Ordronneau, H. Nitadori, I. Photochromic metal complexes: photoregulation of both the nonlinear optical and luminescent properties, Inorg. Chem. 51 (2012) 5627-5636.

[15] D.R. Kains, P.G. Lacroix, M.A. Ratner, T.J. Marks, Electronic structure and quadratic hyperpolarizabilities in organotransition-metal chromophores having weakly coupled 7r-networks. unusual mechanisms for second-order response, J. Am. Chem. Soc. 116 (1994) 10089-10102.

[16] O. Maury, L. Viau, K. Sénéchal, B. Corre, J.P. Guégan, T. Renouard, I. Ledoux, J. Zyss, H. Le Bozee, Synthesis, linear, and quadratic-nonlinear optical properties of octupolar D_3 and D_{2d} bipyridyl metal complexes, Chem. Eur. J. 10 (2004) 4454-4466.

[17] A. Trujillo, M. Fuentealba, D. Carrillo, C. Manzur , I. Ledoux-Rak , J. R. Hamon, J.Y. Saillard, Synthesis, spectral, structural, second-order nonlinear optical properties and theoretical studies on new organometallic donor−acceptor substituted Nickel(II) and Copper(II) unsymmetrical schiff-base complexes, Inorg.

Chem. 49 (2010) 2750-2764.

[18] T. Le Bouder, O. Maury, A. Bondon, K. Costuas, E. Amouyal, I. Ledoux, J. Zyss, H. Le Bozee, Synthesis, photophysical and nonlinear optical properties of macromolecular architectures featuring octupolar tris(bipyridine) Ruthenium(II) moieties: evidence for a supramolecular self-ordering in a dentritic structureJ. Am. Chem. Soc. 125 (2003) 12284-12299.

[19] X.X. Sun, N.N. Ma, X.J. Li, S.L. Sun, H.M. Xie, Y.Q. Qiu, Computational study: How redox affect the nonlinear optical properties of donor substituted heteroleptic bis-tridentate Ru(II) complexes? J. Mol. Graphics. Modell. 38 (2012) 248-255.

[20] F. Tessore, D. Roberto, R. Ugo, M. Pizzotti, Terpyridine Zn(II), Ru(III), and Ir(III) complexes: the relevant role of the nature of the metal ion and of the ancillary ligands on the second-order nonlinear response of terpyridines carrying electron donor or electron acceptor groups, Inorg. Chem. 44 (2005) 8967-8978.

[21] Y. Maeda, H. Hashimoto, T. Nishioka. Sulfur containing platinum(II) complexes with N obtained by reactions of a hydrosulfido complex, Dalton Trans. 41 (2012) 12038-12047

[22] D. Espa, L. Pilia, L. Marchio, M. Pizzotti, N. Robertson, F. Tessore, Naphthoxaphospholes as examples of fluorescent phospha-acenes, Dalton Trans. 41 (2012) 12106-12113.

[23] J.J. Novoa, P.W. Stephens, M. Weerasekare, W.W. Shum, J.S. Miller, The tetracyanopyrazinide dimer dianion, $[TCNP]_2^{2-}$. 2-electron 8-center bonding, J. Am. Chem. Soc. 131 (2009) 9070-7075.

[24] G. Frenking, N. Fröhlich, The nature of the bonding in transition-metal compounds, Chem Rev. 100 (2000) 717-774.

[25] I. Asselberghs, K. Clays, A. Persoons, M.D. Ward, J. McCleverty, Switching of molecular second-order polarisability in solution, J. Mater. Chem. 14 (2004) 2831-2839.

[26] V. Aubert, V. Guerchais, E. Ishow, K. Hoang-Thi, I. Ledoux, K. Nakatani, H. Le Bozec, Efficient photoswitching of the nonlinear optical properties of dipolar photochromic Zinc(II) Complexes, Angew. Chem. Int. Ed. 47 (2008) 577-580.

[27] E. Cariati, C. Dragonetti, E. Lucenti, F. Nisic, S. Righetto, D. Roberto, E. Tordin, An acido-triggered reversible luminescent and nonlinear optical switch based on a substituted styrylpyridine: EFISH measurements as an unusual method to reveal a protonation–deprotonation NLO contrast, Chem. Commun. 50 (2014) 1608-1610.

[28] W.Y. Wang, N.N. Ma, S.L. Sun, Y.Q. Qiu, Redox control of ferrocene-based complexes with systematically extended p-conjugated connectors: switchable and tailorable second order nonlinear optics, Phys. Chem. Chem. Phys. 16 (2014) 4900-4910.

[29] M. Kuss-Petermann, H. Wolf, D. Stalke, O.S. Wenger, Influence of donor–acceptor distance variation on photoinduced electron and proton transfer in Rhenium(I)–phenol dyads, J. Am. Chem. Soc. 134 (2012) 12844-12854.

[30] M.J. Frisch, G.W. Trucks, H.B. Schlegel, G.E. Scuseria, M.A. Robb, J.R. Cheeseman, G. Scalmani, V. Barone, B. Mennucci, G.A. Petersson, H. Nakatsuji, M. Caricato, X. Li, H.P. Hratchian, A.F. Izmaylov, J. Bloino, G. Zheng, J.L. Sonnenberg, M. Hada, M. Ehara, K. Toyota, R. Fukuda, J. Hasegawa, M. Ishida, T. Nakajima, Y. Honda, O. Kitao, H. Nakai, T. Vreven, J.A. Montgomery Jr., J.E. Peralta, F. Ogliaro, M. Bearpark, J.J. Heyd, E. Brothers, K.N. Kudin, V.N. Staroverov, R. Kobayashi, J. Normand, K. Raghavachari, A. Rendell, J.C. Burant, S.S. Iyengar, J. Tomasi, M. Cossi, N. Rega, J.M. Millam, M. Klene, J.E. Knox, J.B. Cross, V. Bakken, C. Adamo, J. Jaramillo, R. Gomperts, R.E. Stratmann, O. Yazyev, A.J. Austin, R. Cammi, C. Pomelli, J.W. Ochterski, R.L. Martin, K. Morokuma, V.G. Zakrzewski, G.A. Voth, P. Salvador, J.J. Dannenberg, S. Dapprich, A.D. Daniels, O. Farkas, J.B. Foresman, J.V. Ortiz, J. Cioslowski, D.J. Fox, Gaussian 09, Revision A. 02, Gaussian, Inc., Wallingford CT, 2009.

[31] C.G. Liu, X.H. Guan, Redox and photoisomerization switching of the second-order optical nonlinearity of a tetrathiafulvalene derivative of spiropyran across five states: a DFT studyPhys. Chem. Chem. Phys. 14 (2012) 5297-5306.

[32] T. Lu, F. Chen, Multiwfn: A multifunctional wavefunction analyzer, J. Comput. Chem. 33 (2012) 580-592.

[33] W. Humphrey, A. Dalke, K. Schulten, VMD: visual molecular dynamics, J. Mol. Graph. 14 (1996) 33-38.

[34] J.R. Rustad, D.A. Dixon, K.M. Rosso, A.R. Felmy, Trivalent ion hydrolysis reactions: a Linear free-energy relationship based on density functional electronic structure calculations, J. Am. Chem. Soc. 121 (1999) 3234-3235.

[35] P. Chopra, L. Carlacci, H.F. King, P.N. Prasad, Ab initio calculations of polarizabilities and second hyperpolarizabilities in organic molecules with extended .pi.-electron conjugation, J. Phys. Chem. 93 (1989) 7120-7130.

[36] P. Karamanis, G. Maroulis, An *ab initio* study of CX_3-substitution (X = H, F, Cl, Br, I) effects on the static electric polarizability and hyperpolarizability of diacetylene, J. Phys. Org. Chem. 24 (2011) 588-599.

[37] H. Iikura, T. Tsuneda, T. Yanai, K. Hirao, A long-range correction scheme for generalized-gradient-approximation exchange functionals, J. Chem. Phys. 115 (2001) 3540-3544.

[38] Y.X. Zhang, B. Champagne, Theoretical insight into the second-order NLO response of the bis{4-[2-(4-pyridyl)ethenyl]benzoato}-zinc(II) metal−organic framework, J. Phys. Chem. C 116 (2012) 21973-21981.

[39] M. Makowska-Janusik, O. Gladii, A. Kassiba, J. Bouclé, N. Herlin-Boime, Cluster approach to model titanium dioxide as isolated or organic dye sensitized nanoobjects, J. Phys. Chem. C 118 (2014) 6009-6018.

[40] B. Champagne, J. Guthmuller, F. Perreault, A. Soldera, Theoretical design of the molecular structure of bent-core mesogens with large second-order nonlinear optical properties, J. Phys. Chem. C 116 (2012) 7552-7560.

[41] I.W. Bulik, R. Zaleśny, W. Bartkowiak, J.M. Luis, B. Kirtman, G.E. Scuseria, A. Avramopoulos, H. Reis, M.G. Papadopoulos, Performance of density functional theory in computing nonresonant vibrational (hyper)polarizabilities, J. Comp. Chem. 34 (2013) 1775-1784.

[42] Y. Tawada, T. Tsuneda, S. Yanagisawa, T. Yanai, K. Hirao, A long-range-corrected time-dependent density functional theory, J. Chem. Phys. 120 (2004) 8425-8433.

[43] K.Y. Suponitsky, Y. Liao, A.E. Masunov, Electronic Hyperpolarizabilities for donor−acceptor molecules with long conjugated bridges: calculations versus experiment, J. Phys. Chem. A 113 (2009) 10994-11001.

[44] T. Yanai, D.P. Tew, N.C. Handy, A new hybrid exchange–correlation functional using the coulomb-attenuating method (CAM-B3LYP), Chem. Phys. Lett. 393 (2004) 51-57.

[45] J. Lin, K.C. Wu, M.X. Zhang, A new hybrid DFT approach to electronic excitation and first hyperpolarizabilities of transition metal complexes, J. Comput. Chem. 30 (2009) 2056-2063.

[46] A. Plaquet, M. Guillaume, B. Champagne, L. Rougier, F. Mancüois, V. Rodriguez, J.L. Pozzo, L. Ducasse, F. Castet, Investigation on the second-order nonlinear optical responses in the keto−enol equilibrium of anil derivatives, J. Phys. Chem. C 112 (2008) 5638-5645.

[47] F. Furche, R. Ahlrichs, "Adiabatictime-dependent density functional methods for excited state properties," J. Chem. Phys. 117(2002) 7433-7447.

Table 1

Selected bond lengths (Å), bond angle (°), difference between single and double bond lengths (BLA) values and wiberg bond index (WBI) values obtained at the B3LYP/6-31G(d)/LanL2DZ level.

Complex	**1a-H**	**2a-H**	**2a-H (PCM)[c]**	**3a-H**	**1a**	**2a**	**3a**
Re−N1	2.201	2.203(2.205)[a]	2.202	2.204	2.208	2.200	2.202
Re−N2	2.207	2.207(2.181)[a]	2.207	2.207	2.213	2.205	2.201
Re−N3	2.216	2.217(2.175)[a]	2.216	2.216	2.212	2.205	2.203
Re−C1	1.932	1.932(1.928)[a]	1.931	1.932	1.929	1.930	1.931
Re−C2	1.938	1.928(1.920)[a]	1.926	1.938	1.941	1.935	1.932
Re−C3	1.932	1.912(1.912)[a]	1.910	1.932	1.930	1.931	1.930
O-H	0.9680	0.9603	-	0.9540	-	-	-
N2−Re−N3	75.12	75.14(75.94)[a]	74.72	75.25	75.31	75.60	75.72
C2−Re−C3	90.53	90.51(91.86)[a]	89.70	90.53	90.59	90.84	90.97
N2−Re−C2	97.14	97.14(97.26)[a]	96.15	97.13	96.91	96.66	96.48
N3−Re−C3	97.10	94.11(94.98)[a]	94.28	97.04	96.99	96.67	96.57
BLA[b]	0.046	0.043	-	0.040	0.030	0.025	0.020
WBI	0.7106	0.7187	-	0.7249	-	-	-

[a] Experimental values from ref. [29]. [b] the corresponding BLA were plotted in the black bold as shown in Fig. 1. [c] the geometrical structures were obtained at the B3LYP/6-31G(d) (LanL2DZ basis set for Re ion) level in the acetonitrile solution

Table 2

Electron density and energy density at the critical point on the basis of atoms in molecules (AIM) theory was performed by Multiwfn 3.5 software.

Complex	Electron density	Energy density
1a-H	0.3488	-0.5277
2a-H	0.3498	-0.5285
3a-H	0.3503	-0.5288

Table 3

Dipole moments and static first hyperpolarizabilities β_{vec} (a.u.) of all complexes have been obtained by two methods. Effect of solvent on static first hyperpolarizabilities has also been obtained by CAM-B3LYP method at the polarizable continuum model (PCM) in the presence of acetonitrile solution.

Complex	Method	μ_x	μ_z	$\|\mu\|$	β_x	β_y	β_z	β_{vec}
1a-H	CAM-B3LYP	5.5	5.8	8.1	-1.7×10^{3}	-6.6×10	4.4×10^{3}	2.0×10^{3}
	CAM-B3LYP (PCM)	5.0	6.5	8.3	-1.5×10^{3}	-8.3×10	5.7×10^{3}	2.2×10^{3}
	LC-BLYP	5.6	5.3	7.8	-9.7×10^{2}	-3.1×10	3.7×10^{3}	1.8×10^{3}
2a-H	CAM-B3LYP	5.3	5.9	8.0	-1.8×10^{3}	-2.6×10^{3}	7.8×10^{3}	4.5×10^{3}
	CAM-B3LYP (PCM)	5.0	6.3	8.1	-1.2×10^{3}	-2.3×10^{2}	1.1×10^{4}	5.9×10^{3}
	LC-BLYP	5.5	5.6	7.9	-8.7×10^{2}	-2.1×10^{2}	9.0×10^{3}	5.8×10^{3}
3a-H	CAM-B3LYP	4.7	6.4	7.9	-2.7×10^{3}	8.1×10	2.2×10^{4}	1.6×10^{4}
	CAM-B3LYP (PCM)	5.4	5.3	7.6	-1.9×10^{3}	1.1×10	1.8×10^{4}	1.7×10^{4}
	LC-BLYP	4.9	5.9	7.7	-1.4×10^{3}	1.5×10	1.2×10^{4}	8.5×10^{3}
1a	CAM-B3LYP	5.1	-9.8	11.1	-4.1×10^{3}	1.9×10^{2}	2.4×10^{4}	-2.3×10^{4}
	CAM-B3LYP (PCM)	5.5	-9.6	11.2	-7.8×10^{2}	-2.1×10^{2}	2.3×10^{4}	-2.0×10^{4}
	LC-BLYP	4.5	-7.4	8.7	-1.2×10^{3}	-9.8×10	1.1×10^{4}	-9.7×10^{3}
2a	CAM-B3LYP	4.2	-14.3	14.9	-7.6×10^{3}	-4.9×10^{3}	1.6×10^{5}	-1.0×10^{5}
	CAM-B3LYP (PCM)	6.1	-18.0	19.0	-2.6×10^{3}	4.3×10	1.2×10^{5}	-1.1×10^{5}
	LC-BLYP	5.1	-14.0	14.9	-5.5×10^{3}	4.2×10	1.0×10^{5}	-9.9×10^{4}
3a	CAM-B3LYP	4.2	-18.7	19.1	-7.9×10^{4}	-4.3×10^{3}	5.2×10^{5}	-5.2×10^{5}
	CAM-B3LYP (PCM)	7.4	-26.8	27	-6.4×10^{3}	-2.5×10^{3}	9.6×10^{4}	-9.4×10^{5}

LC-BLYP	6.3	-22.7	23.6	-2.2×10^{4}	-7.5×10^{3}	2.9×10^{5}	-2.8×10^{5}

Table 4

Wavelengths (λ, nm), excited state transition energies (E_{ge}, eV), oscillator strengths (f_{os}), and major molecular orbital contributions of all complexes calculated using TDDFT method at the CAM-B3LYP/6-31+G(d) (LanL2DZ basis set for Re ion) level in the acetonitrile solution.

Complex	λ/nm	E_{ge}/eV	f_{os}	Major contributions
1a-H	298	4.16	0.7149	H[a]-1→L (68%)
2a-H	299	4.15	1.0424	H-1→L (70%)
3a-H	322	3.85	1.3109	H-3→L (54%), H-1→L(45%)
1a	396	3.13	1.2079	H→L+2 (94%)
2a	446	2.78	0.9098	H→L+2 (80%)
3a	459	2.70	1.4180	H→L+2 (91%)

[a]assignment: H = HOMO, L = LUMO, H-1= HOMO-1, L+1 = LUMO+1, etc.

Table 5

The frequency-dependent β_{vec} (-2ω;ω,ω) values and effect of solvent (in the acetonitrile solution) on frequency-dependent β_{vec} (-2ω;ω,ω) values for all studied complexes have been evaluated by couple-perturbed (CP) DFT method, CAM-B3LYP functional at ω = 1.064 μm (0.0428 eV)

Complex	**1a-H**	**2a-H**	**3a-H**	**1a**	**2a**	**3a**
β (-2ω;ω,ω)	2.0×10^{3}	4.5×10^{3}	1.6×10^{4}	-2.3×10^{4}	-1.5×10^{5}	-9.2×10^{5}
Complex	**1a-H (PCM)**	**2a-H (PCM)**	**3a-H (PCM)**	**1a (PCM)**	**2a (PCM)**	**3a (PCM)**
β (-2ω;ω,ω)	2.2×10^{3}	4.7×10^{3}	1.7×10^{4}	-2.7×10^{4}	-1.8×10^{5}	-9.6×10^{5}

Figure captions

Fig. 1. The geometric structures of the studied complexes (**1a-H**, **2a-H**, and **3a-H** are the protonated complexes, while **1a**, **2a**, and **3a** are the deprotonated complexes)

Fig. 2 Local orbital coupling of for the Re-N1 (N2 or N3) fragment of complexes **2a-H** and **2a**

Fig. 3. The electrostatic potentials of the studied complexes **1a** to **3a** (red regions indicate negative charge, while blue regions represent positive charge)

Fig. 4. Relationship between the β_{vec} value and the corresponding E_{ge} values for the all complexes (a: the protonated species, b: the deprotonated species)

Fig. 5. Simulated absorption spectra of all complexes (**a**: the protonated species, **b**: the deprotonated species) calculated at the CAM-B3LYP/6-31+G(d) (LanL2DZ basis set for Re ion) level.

Fig. 6. Molecular orbitals of all complexes involved in the dominant electron transitions obtained at the CAM-B3LYP /6-31+G(d)/ LanL2DZ level.

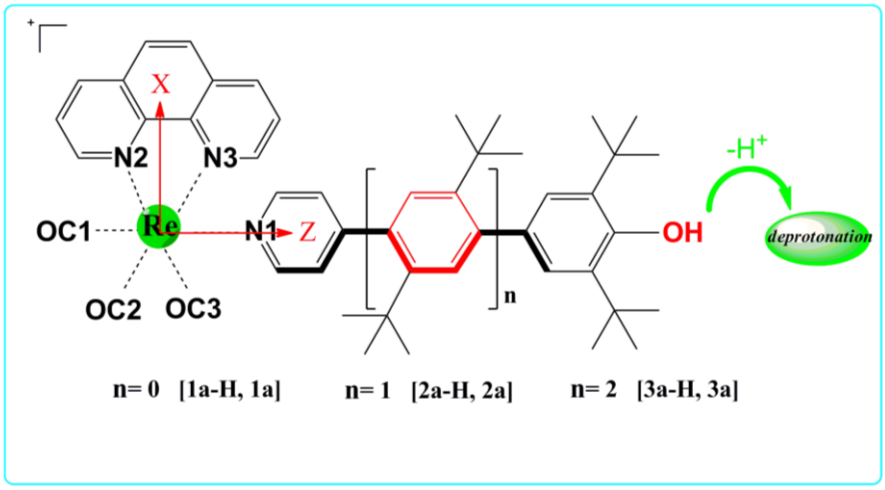

Fig. 1. The geometric structures of the studied complexes (**1a-H**, **2a-H**, and **3a-H** are the protonated complexes, while **1a**, **2a**, and **3a** are the deprotonated complexes)

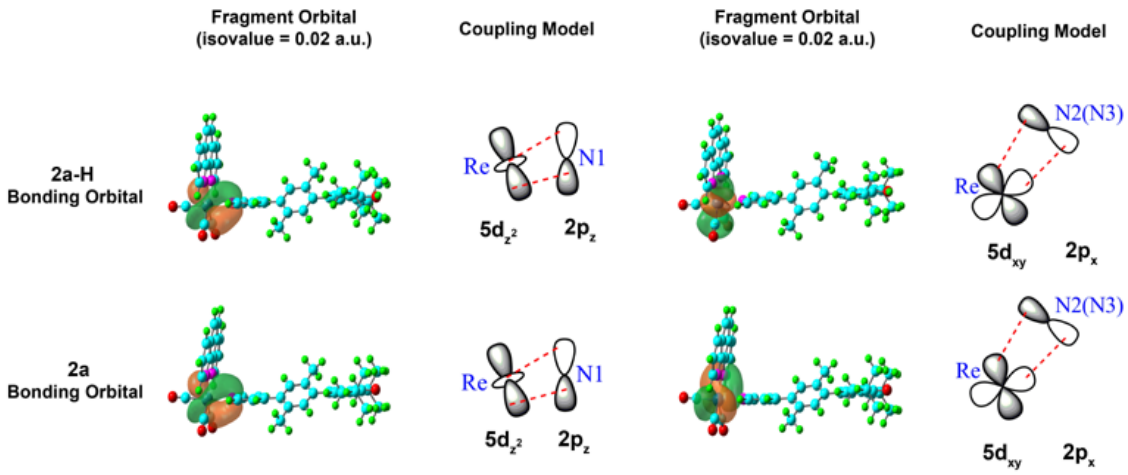

Fig. 2 Local orbital coupling of for the Re-N1 (N2 or N3) fragment of complexes **2a-H** and **2a**

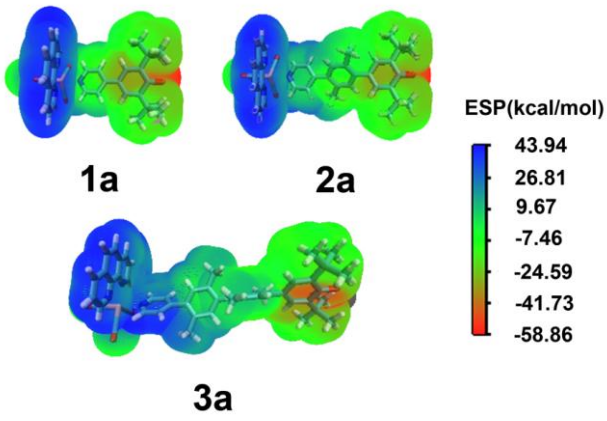

Fig. 3. The electrostatic potentials of the studied complexes **1a** to **3a** (red regions indicate negative charge, while blue regions represent positive charge)

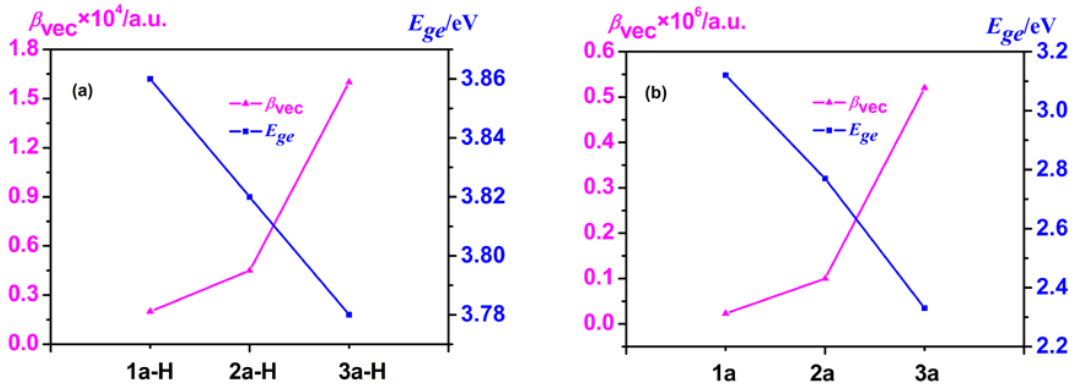

Fig. 4. Relationship between the β_{vec} value and the corresponding E_{ge} values for the all complexes (a: the protonated species, b: the deprotonated species)

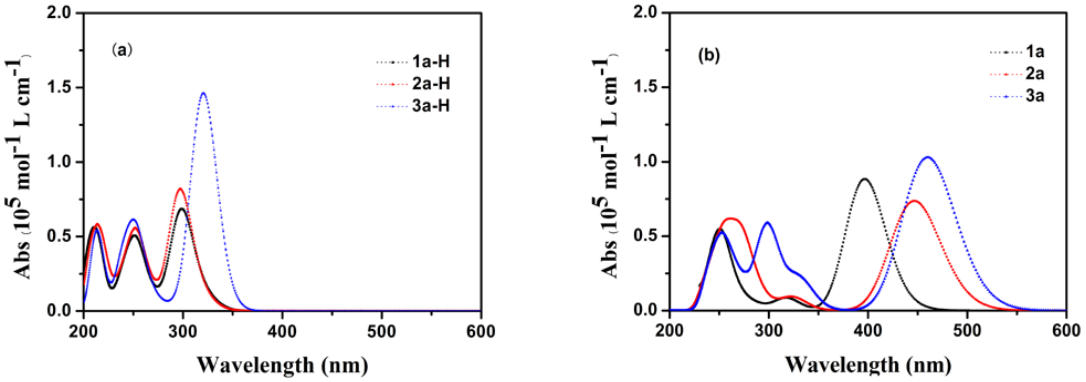

Fig. 5. Simulated absorption spectra of all complexes (**a**: the protonated species, **b**: the deprotonated species) calculated at the CAM-B3LYP/6-31+G(d) (LanL2DZ basis set for Re ion) level.

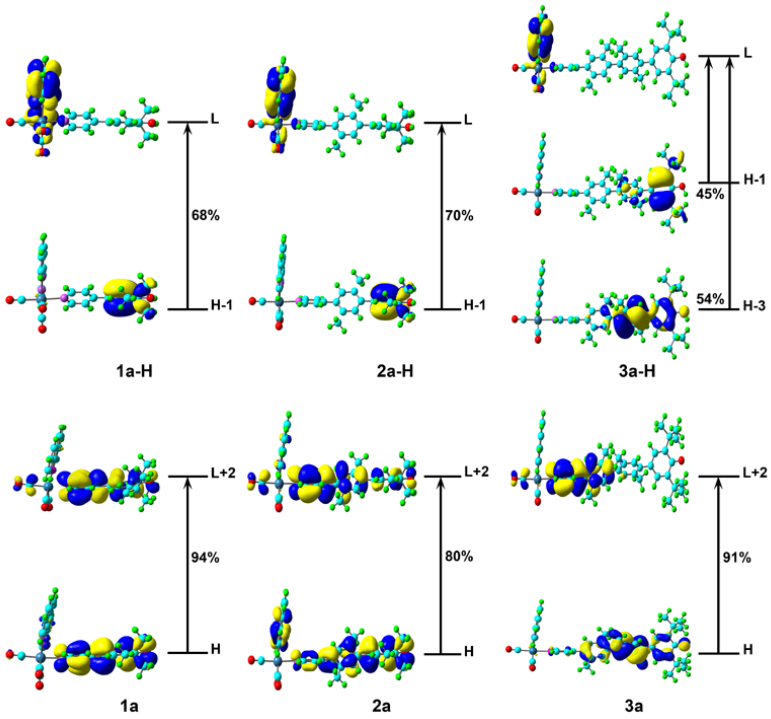

Fig. 6. Molecular orbitals of all complexes involved in the dominant electron transitions obtained at the CAM-B3LYP /6-31+G(d)/ LanL2DZ level.